European Journal of Pharmaceutical Sciences 159 (2021) 105698

Contents lists available at ScienceDirect

European Journal of Pharmaceutical Sciences

journal homepage: www.elsevier.com/locate/ejps

Mucoadhesive nanostructured lipid carriers as a cannabidiol nasal delivery system for the treatment of neuropathic pain

Ananda Pulini Matarazzo [a], Lívia Maria Silvestre Elisei [b], Flávia Chiva Carvalho [a], Rudy Bonfílio [a], André Luís Morais Ruela [c], Giovane Galdino [b], Gislaine Ribeiro Pereira [a,*]

[a] Faculty of Pharmaceutical Sciences, Federal University of Alfenas (UNIFAL-MG), Alfenas, Minas Gerais, Brazil
[b] Science of Motricity Institute, Federal University of Alfenas (UNIFAL-MG), Alfenas, Minas Gerais, Brazil
[c] Pharmacy School, Federal University of Ouro Preto (UFOP), Ouro Preto, Minas Gerais, Brazil

ARTICLE INFO

Keywords:
Cannabidiol
Nanostructured lipid carriers
Mucoadhesion
Nasal administration
Neuropathic pain

ABSTRACT

The therapeutic potential of cannabidiol (CBD) has been explored to treat several pathologies, including those in which pain is prevalent. However, the oral bioavailability of CBD is low owing to its high lipophilicity and extensive first-pass metabolism. Considering the ability of the nasal route to prevent liver metabolism and increase brain bioavailability, we developed nanostructured lipid carriers (NLCs) for the nasal administration of CBD. We prepared particles with a positively charged surface, employing stearic acid, oleic acid, Span 20®, and cetylpyridinium chloride to obtain mucoadhesive formulations. Characterisation of the CBD-NLC dispersions showed uniform nano-sized particles with diameters smaller than 200 nm, and high drug encapsulation. The mucoadhesion of cationic particles has been related to interactions with negatively charged mucin. Next, we added *in-situ* gelling polymers to the CBD-NLC dispersion to obtain a CBD-NLC-gel. A thermo-reversible *in-situ* forming gel was prepared by the addition of Pluronics®. CBD-NLC-gel was characterised by its gelation temperature, rheological behaviour, and mucoadhesion. Both formulations, CBD-NLC and CBD-NLC-gel, showed high mucoadhesion, as assessed by the flow-through method and similar in vitro drug release profiles. The in vivo evaluation showed that CBD-NLC dispersion (without gel), administered intranasally, produced a more significant and lasting antinociceptive effect in animals with neuropathic pain than the oral or nasal administration of CBD solution. However, the nasal administration of CBD-NLC-gel did not lessen mechanical allodynia. These findings demonstrate that *in-situ* gelling hydrogels are not suitable vehicles for highly lipophilic drugs such as CBD, while cationic CBD-NLC dispersions are promising formulations for the nasal administration of CBD.

1. Introduction

Chemotherapy-induced peripheral neuropathy (CIPN) is considered a common adverse effect in cancer patients undergoing chemotherapy, and 40–80% of patients undergoing chemotherapy develop CIPN in the first 3–6 months of treatment (Blanton et al., 2019; Starobova and Vetter, 2017). The treatment of CIPN with common painkillers is unsatisfactory. Therefore, several studies have been carried out using cannabidiol (CBD; Fig. 1) in the treatment of this pain (Blanton et al., 2019; Brenneman et al., 2019; De Gregorio et al., 2019).

CBD is a phytocannabinoid found in the *Cannabis sativa* plant, and belongs to a group of natural, endogenous, and synthetic compounds called cannabinoids. These compounds modulate several important physiological functions in organisms, such as locomotion, memory, pain perception, food intake, and inflammatory reactions (Fasinu et al., 2016). This phytocannabinoid is a highly lipophilic molecule (logP = 6.64) and is sparingly soluble in aqueous media. It is classified as a Class II substance according to the Biopharmaceutical Classification System (Gaston and Friedman, 2017; Cherniakov et al., 2017; Paudel et al., 2010). The low aqueous solubility of CBD, associated with the extensive metabolism that it undergoes in the first passage through the liver, makes its oral bioavailability low and variable (6–13%) (WHO, 2018; Cherniakov et al., 2017).

Considering the inconveniences of oral CBD administration, we developed a nasal delivery system for CBD. The nasal route prevents first-pass hepatic metabolism and avoids the blood–brain barrier. The nasal epithelium, with its high permeability to small and lipophilic molecules, has a large absorption surface, promoting rapid absorption of

* Corresponding author.
E-mail address: gislaine.pereira@unifal-mg.edu.br (G.R. Pereira).

https://doi.org/10.1016/j.ejps.2020.105698
Received 5 September 2020; Received in revised form 4 December 2020; Accepted 28 December 2020
Available online 3 January 2021

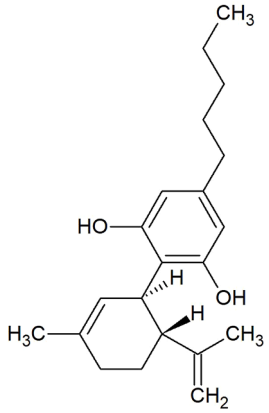

Fig. 1. Structure of cannabidiol ($C_{21}H_{30}O_2$; Molecular weight = 314.45 g•mol^{-1}).

the drug (Bruni et al., 2018; Cunha et al., 2017). Consequently, this administration route has frequently been explored, especially for drugs acting on the central nervous system (Chatterjee et al., 2019; Costa et al., 2019). The main limitation of the nasal route is mucociliary clearance, which causes low drug availability by shortening the residence time of the formulation on the nasal epithelium. The formulations must therefore be designed to increase their residence time in the nasal cavity. This challenge may be overcome using formulations with mucoadhesive properties (Martins et al., 2019). Although the physicochemical characteristics of CBD hinder the development of mucoadhesive nasal formulations, the use of nanocarriers is a promising strategy for the administration of this compound.

Nanostructured lipid carriers (NLCs) are colloidal particles, composed of a biodegradable and biocompatible lipid matrix capable of encapsulating highly lipophilic drugs, with low toxicity to the nasal mucosa. After administration via the nasal pathway, NLCs promote drug targeting of the brain increasing the bioavailability and half-life of the drug (Beloqui et al., 2016; Deepak et al., 2019). When incorporated into NLCs, the bioavailability of the drug is increased as it is protected from degradation and the efflux that would return it to the nasal cavity (Costa et al., 2019; Cunha et al., 2017; Gadhave and Kokare, 2019).

In this study, we develop a CBD nasal delivery system composed of NLCs loaded with this bioactive compound. To increase the bioadhesiveness of this formulation, we employed two strategies: (i) obtaining particles with a positively charged surface, and (ii) adding an *in-situ* gelling polymer into the NLC dispersion. The formulations were characterised in vitro, and an in vivo assay was used to evaluate the antinociceptive effects of these nasal drug delivery systems when administered to mice with neuropathic pain induced by chemotherapy.

2. Materials and methods

2.1. Materials

CBD (≥ 98%) was purchased from THC-Pharm-GmbH (Frankfurt, Germany). Stearic acid (≥ 95%), oleic acid (≥ 99%), cetylpyridinium chloride (≥ 98%), Span 20® (≥ 44%), Pluronic F68®, and Pluronic F127® were purchased from Sigma-Aldrich (Steinheim, Germany). Paclitaxel (Ontax® 100 mg, Libbs Farmacêutica), as a solution for injection, was purchased from Libbs (Embu das Artes, Brazil). All other reagents used were of chromatographic grade.

2.2. High performance liquid chromatography analysis

For the quantification of CBD, an analytical method was developed and validated following the International Council for Harmonisation of Technical Requirements for Pharmaceuticals for Human Use and Agência Nacional de Vigilância Sanitária (ICH, 2005; Brasil, 2017). The analyses were performed using high performance liquid chromatography (HPLC) Prominence equipment (Shimadzu®, Kyoto, Japan) and a C18 column, 150.0 × 4.6 (id) with a 5-μm particle size (LiChrospher® 100 RP-18 endcapped, Merck). The mobile phase was a mixture of acetonitrile, methanol, and water (50:30:20 v/v/v). The flow rate of the mobile phase was 1.0 mL•min^{-1}, the injection volume was 50 μL, and UV detection was performed at 208 nm. The time retention of CBD was 7.78 min. The linearity of the method was demonstrated over a range of 1.0–20.0 μg•mL^{-1} (correlation coefficient = 0.9979). The limit of quantification and limit of detection were 0.167 and 0.055 μg•mL^{-1}, respectively. The precision of the analytical method was illustrated by the low variability of the data (<5%), and the accuracy remained in the range of ± 5%.

2.3. NLC preparation

CBD-loaded NLCs (CBD-NLC) were obtained using the hot microemulsion technique (Gasco, 1993). The NLCs were prepared using stearic acid (1.25%) as a solid lipid and oleic acid (0.75%) as a liquid lipid. To obtain particles with a positively charged surface, cetylpyridinium chloride (0.05%) was employed as an active surfactant and Span 20® (0.25%) as a co-surfactant. A mixture of stearic acid, oleic acid, cetylpyridinium chloride, and Span 20® was heated to 85 °C, after which CBD (150 mg) was added. The microemulsion is only formed after heating and stirring (500 rpm), when 300 μL of purified water is added and a transparent system is obtained. The hot microemulsion was dripped into 20 mL of purified ice water (2–4 °C) under vigorous stirring (13,400 rpm for 10 min, IKA T25 Ultra-Turrax®) to form the CBD-NLC dispersion. Unloaded-NLCs were prepared as controls using the same method without adding CBD.

2.4. NLC characterisation

2.4.1. Particle size, polydispersity index, and zeta potential

The average hydrodynamic particle size, polydispersity index (PdI), and zeta potential were determined by dynamic light scattering (DLS) using a Zetasizer Nano ZS analyser (Malvern Instruments, UK) with a 633-nm laser. All the samples were diluted (1:100) in purified water and the measurements were performed at 25 °C. The zeta potential measurements were performed in water with a pH adjusted to 6.0, and conductivity adjusted to approximately 50 μS•cm^{-1} (20 °C) using sodium chloride solution (10 mmol•L^{-1}).

2.4.2. Entrapment efficiency and drug loading

Drug entrapment efficiency (EE) and drug loading (DL) refer to the amount (%) of drug encapsulated by the NLCs. EE and DL were indirectly determined by the ultrafiltration/centrifugation method using Amicon® ultrafiltration devices (Millipore, 50-kD cut-off). One millilitre of freshly prepared CBD-NLC dispersion was added to the upper part of the device and centrifuged at 3400 rpm for 30 min. The CBD-NLC retained on the filter was washed three times to remove any free drug. The amount of CBD in the filtered pool (free drug) was determined by HPLC. The amount of CBD in the dispersion (total drug) was determined by dissolving an aliquot of the dispersion in methanol followed by HPLC. The EE (%) and DL (%) were calculated using Eqs. (1) and 2:

$$EE\ (\%) = (total\ drug - free\ drug) / (total\ drug) \times 100 \quad (1)$$

$$DL\ (\%) = (total\ drug - free\ drug) / (weight\ of\ lipids) \times 100 \quad (2)$$

2.4.3. Assessment of NLC mucoadhesion by zeta potential measurement

The mucoadhesion of NLC was tested by assessing the effects of the mucin solutions on particle zeta potential (Shen et al., 2009). Aliquots of the NLC dispersion (10 μL) were placed in contact with mucin solutions

(10 μL) at concentrations of 0.025, 0.05, 0.1, 0.25, 0.5, 1.0, 2.0, 3.0, 4.0, and 5.0 mg•mL^{-1}. The mixtures were diluted to a final volume of 10 mL with purified water, and the zeta potential of each diluted mixture was measured.

2.4.4. Atomic force microscopy

The nanoparticles were visualised by atomic force microscopy (AFM) using a Park® microscope (model NX10). The images were obtained in non-contact operating mode, with a silicon-type probe (model NSC15) and a cantilever resonance frequency of 277.39 kHz. Aliquots (10 μL) of the unloaded-NLC and CBD-NLC dispersions were deposited on mica plates and dried at room temperature.

2.4.5. Differential scanning calorimetry

Differential scanning calorimetry (DSC) measurements were performed using a Syrius 3500 calorimeter (Netzsch®, Germany). Samples of freeze-dried NLCs (unloaded-NLC and CBD-NLC), stearic acid (solid lipid), CBD, and mannitol (cryoprotectant used in the freeze-drying process) were weighed (6 mg) and placed in sealed aluminium pans. DSC curves were recorded from 50 to 250 °C at a heating rate of 10 °C•min^{-1} under a nitrogen atmosphere (50 mL•min^{-1}).

2.4.6. Powder X-ray diffraction

The NLCs dispersions (unloaded-NLC and NLC—CBD) were subjected to freeze-drying using mannitol as a cryoprotectant. The diffraction patterns of the NLC samples, stearic acid, CBD, and mannitol were obtained using an Ultima IV (type II) diffractometer (Rigaku®, Japan) under the following conditions: room temperature (293 K), CuKα radiation (1.5418 Å) generated at 40 kV and 30 mA, a 10-mm wide slit, continuous scan mode with a 0.02° 2θ step size, a scan speed of 1° 2θ•min^{-1}, and an angular range of 5–35° in 2θ.

2.4.7. Fourier transform infrared–attenuated total reflectance

Fourier transform infrared (FTIR)–attenuated total reflectance spectra of the freeze-dried NLCs (unloaded-NLC and CBD-NLC), stearic acid, CBD, and mannitol were obtained using a FTIR spectrophotometer, model Affinity-1 (Shimadzu®, Japan), coupled with an attenuated total reflectance sampling accessory with ZnSe waveguides (Pike Technologies®, USA). The spectra were recorded in transmittance mode at room temperature, using 32 scans per analysis at a resolution of 4.0 cm^{-1}, in a range of 4000–600 cm^{-1}.

2.5. NLC-gel

2.5.1. Gelation study of NLC dispersions

Initially, NLC-gels were prepared by dispersing Pluronic F127® and Pluronic F68® in proportions of 19:1, 18:2, and 17:3 using the cold method. For this, 20% (w/v) of Pluronic was dispersed in the NLC dispersion in an ice bath with stirring for 20 min. Then, the formulations were placed in a water bath, where the temperature was increased by 1 °C•min^{-1} until the gelation temperature was observed. A thermometer was used to monitor the temperature changes of the formulations. *Ti* (temperature at the start of gelation) and *Tg* (temperature of total gelation of the system) were recorded.

2.5.2. Texture and mucoadhesion analysis of the NLC-gels

Texture profile analysis and mucoadhesive strength determination were performed on the NLC-gels using a TA-XT plus texture analyser (Stable Micro Systems, Surrey, England) (Ruela et al., 2016; Colombo et al., 2018). For texture profile analysis, the samples were conditioned in 50-mL centrifuge tubes (Falcon, BD®, Franklin Lakes, NJ, USA), and a 10-mm diameter analytical probe was descended at a constant speed (1 mm•s^{-1}) until the sample was reached. Then, the probe continued to a depth of 10 mm within the sample. Next, the probe was returned to the surface at a speed of 0.5 mm•s^{-1} and, after 5 s, a second compression was started. The test provided a force–time curve from which it was possible to calculate mechanical parameters, such as hardness, compressibility, and cohesiveness (Fig. 1SA).

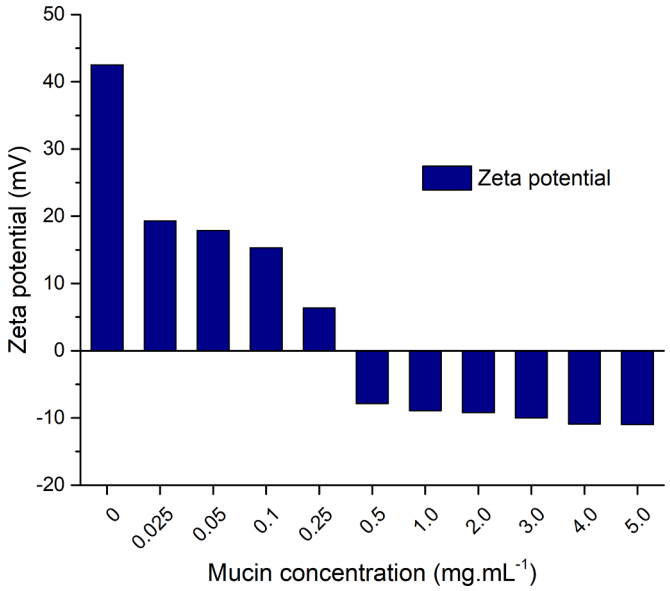

Fig. 2. Measurement of the zeta potential of CBD-NLC after adding different concentrations of mucin (0.025–5.0 mg•mL^{-1}).

Mucoadhesive strength was determined by measuring the strength required to detach samples maintained in contact with a porcine intestinal mucosa (used as a mucosa model). Fresh porcine intestinal mucosa was obtained from healthy pigs at a local slaughterhouse (Alfenas, Brazil). The porcine intestinal mucosa was washed under running water, cut into appropriately sized pieces for analysis, and washed again with saline solution. The mucosa was attached to the analytical probe with the lumen of the intestinal mucosa exposed to the external environment. The formulations were placed below the probe, and the test was performed by lowering the probe at a constant speed (0.5 mm•s^{-1}) until the mucosa and formulation made contact. The mucosa and samples were kept in contact for 60 s without the application of any force. Then, the probe was removed at 0.5 mm•s^{-1} until the two surfaces were completely separated. The force required for detachment was recorded. During the analyses, a force–time curve was created, and the work of adhesion and peak adhesion were calculated to describe the mucoadhesive characteristics of the formulations (Fig 1SB). All the analyses were performed on samples placed in a water bath at 37 ± 1 °C to assure sample gelation during the tests.

2.6. Mucoadhesion measurements using the flow-through method

The mucoadhesion of CBD-NLC and CBD-NLC-gel was also evaluated using the flow-through method (Jiang et al., 2017). The analyses were performed using porcine intestinal mucosa, prepared as previously described. The mucosa was placed in a cylindrical tube, which was cut longitudinally in half and fixed at an angle of 45° to facilitate flow. Forty microlitres of the samples were dropped onto the mucosa. To simulate nasal fluid under normal conditions, a flow of artificial nasal fluid [aqueous solution; pH 5.7; consisting of 2.0% (w/v) mucin, 0.745% (w/v) NaCl, 0.129% (w/v) KCl, and 0.032% (w/v) $CaCl_2$] was maintained for 5 min to circulate the surface of the mucosal tissue at a rate of 1 mL•min^{-1}, controlled by a peristaltic pump (Masterflex L/S Series Peristaltic Pumps, United States) (Fig 2S). NLCs with low adhesion force to the mucosal membrane were washed off, and the drug concentration in the eluted solution was quantified by HPLC. Then, the amount of drug retained on the mucosa was determined as the difference between the amount applied to the mucosa and the amount eluted in the artificial nasal fluid solution. The test was performed for the CBD-NLC and

CBD-NLC-gel samples. CBD solution in water with 5% (w/v) Tween 80 was used as a positive control. All the samples had a CBD concentration of 7.5 mg•mL^{-1}.

2.7. Rheology

The rheological behaviours of the CBD-NLC and CBD-NLC-gel were analysed at 25 °C and 37 °C, using an R/S-controlled stress rheometer (Brookfield Engineering Laboratories, Middleboro, MA) and Rheocalc T1.2.19 software. For the analyses at 25 °C, the CP-40 spindle was used, and for the analyses at 37 °C, the CP-52 spindle was used.

The measurements were carried out at progressively higher rotation speeds to obtain ascendant curves. The procedure was then performed in the opposite direction, and descendant curves were obtained. From the results, consistency index values were calculated, according to the Ostwald-deWaele model (Power Law), as described below:

$$\tau = K\,\gamma^{\eta} \quad (3)$$

where τ is the shear stress (D•cm^{-2}), K is the flow consistency index (centipoise, cP), γ is the shear rate (s^{-1}), and η is the flow index. Data adjustment was determined by the coefficient of determination (r^2). For a Newtonian fluid, η = 1; for a pseudoplastic fluid, η < 1.

2.8. In vitro release studies

The in vitro release of CBD from CBD-NLC and CBD-NLC-gel was performed using the USP II apparatus (paddle) in a Nova Etica 299/6 dissolution test system (São Paulo, Brazil). Isotonic phosphate buffer (20 mM, pH 6.8) containing 5% (w/v) Tween 80 was used as the release medium to assure sink conditions. A 1-mL sample (CBD-NLC or CBD-NLC-gel) was placed into each vessel containing 900 mL of release medium, stirred at 100 rpm, and maintained at 37 ± 1 °C. At predetermined time intervals (5, 10, 15, 30, 45, 60, and 90 min), 2-mL aliquots were withdrawn, filtered through 0.1-μm membranes, and the amount of CBD released was determined by HPLC.

2.9. In vivo studies

2.9.1. Animals

Male Swiss mice (8–10 weeks old at the beginning of the experiment) from our breeding colony at the Federal University of Alfenas, Alfenas, Brazil, were used. Mice were housed individually in standard hanging cages, at 22 ± 1 °C and 50% ± 5% relative humidity, using a reversed 12/12 h light/dark cycle with the lights turning on at 7:30 p.m. The animals were provided with standard rodent food and tap water ad libitum. All experiments were conducted between 9:00 a.m. and 5:00 p.m. The present study was conducted with the approval of the Animal Use Ethics Committee at the Federal University of Alfenas (protocol number 33/2018). Furthermore, all experiments were performed in accordance with the International Association for the Study of Pain guidelines on the use of laboratory animals (Zimmermann, 1983).

2.9.2. Model of neuropathic pain induced by chemotherapy

To induce neuropathic pain, the animals received paclitaxel (PTX) intraperitoneally, at a dose of 1 mg•kg^{-1} body weight, every other day for 8 days (four injections in total) (Sekiguchi et al., 2018)

2.9.3. Administration pathways

2.9.3.1. Nasal administration. To evaluate the effects of the nasal administration of CBD on the treatment of neuropathic pain, the test formulations (CBD-NLC and CBD-NLC-gel), the control (CBD solution), and the respective formulation vehicles were intranasally administered. Before nasal administration, the animals were acclimated to restraint by the experimenter to reduce stress. After that, the animals were held by the skin in the cervical region and kept in a dorsal position at an angle of 45°. Approximately 6 μL of formulation was pipetted next to each nostril of the animal to be inhaled, and after 3 s the procedure was repeated (Hanson et al., 2013).

2.9.3.2. Oral administration. The control (CBD solution) and its vehicle were also administered orally. Oral administration was carried out using the gavage method. Gavage was performed with a volume of approximately 0.1 mL/10 g, at a concentration of 5 mg•kg^{-1}.

2.9.4. Assessment of nociceptive threshold

The von Frey filament test (Stoeling, Wood Dale, IL, USA) was used to measure the mechanical nociceptive threshold. For this test, the mice were placed on an elevated wire mesh platform in individual glass compartments, and were allowed to acclimate for at least 60 min. A mechanical stimulus was applied to the middle of the plantar surface, using a series of von Frey filaments with increasing bending forces (0.16, 0.4, 0.6, 1.4, and 2.0 g), and the pressure value was recorded at paw withdrawal. The results reported for the test represent the mean values of three consecutive tests performed at intervals of 3 min.

2.9.5. Motor performance test

Motor performance was evaluated by time spent walking on a rotating rod (13 rpm) (Rota-rod, Bonther, Brazil) for 2 min (cut-off time), as previously described (Dunham and Miya, 1957). Swiss male mice without (control) and with neuropathic pain underwent training sessions for 3 days prior to testing. Motor performance was analysed immediately before (basal) and 30 min, 1:30, 2:30, and 24 h after the administration of the CBD formulations (CBD-NLC, CBD-NLC-gel, or CBD solution intranasally, and CBD solution orally).

2.9.6. Experimental procedure

Initially, the mechanical nociceptive threshold was measured (baseline), and new measurements were taken on the 4th, 7th, 14th, 21st, and 28th days after PTX injection, to assess the peak of nociception for later treatment with CBD. The animals were then randomly divided into the following groups: mice subjected to neuropathic pain induced by PTX (NP) and mice that received the PTX vehicle ($NP_{control}$).

We investigated which dose of CBD would promote analgesia in the animals. For this, a dose-response (2.5 and 5 mg•kg^{-1}) experiment was performed to assess the effect of oral CBD solution on the 14th day of neuropathic pain. Thus, the mice were randomly divided into following groups (n = 6): NP + CBD: mice with neuropathic pain that received CBD solution (5 mg•kg^{-1}) orally; $NP_{control}$ + CBD: mice without neuropathic pain that received CBD solution (5 mg•kg^{-1}) orally.

For nasal administration, the groups were as follows: NP + CBD: mice with neuropathic pain that received CBD solution (5 mg•kg^{-1}) intranasally; $NP_{control}$ + CBD: mice without neuropathic pain that received CBD solution intranasally; NP + CBD-NLC: mice with neuropathic pain that received CBD-NLC (equivalent to 5 mg•kg^{-1} of CBD) intranasally; $NP_{control}$ + CBD-NLC: mice without neuropathic pain that received CBD-NLC intranasally; NP + CBD-NLC-gel: mice with neuropathic pain that received CBD-NLC-gel (equivalent to 5 mg•kg^{-1} of CBD) intranasally; $NP_{control}$ + CBD-NLC-gel: mice without neuropathic pain that CBD-NLC-gel intranasally; Furthermore, control groups were also used to assess the effects of the vehicle. In the groups of animals that received the drug or vehicle, new measurements of the nociceptive threshold were taken at intervals 30 min, 1:30, 2:30, 3:30, 4:30, 5:30, 24, and 48 h after administration on the 14th day of neuropathic pain.

Finally, to evaluate the effect of CBD on the motor performance of the animals, the following groups were used (n = 5): NP + CBD_{oral}; NP + $CBD_{nasal;}$ NP + CBD-NLC; NP; and $NP_{control.}$ This procedure is described in Section 2.9.5.

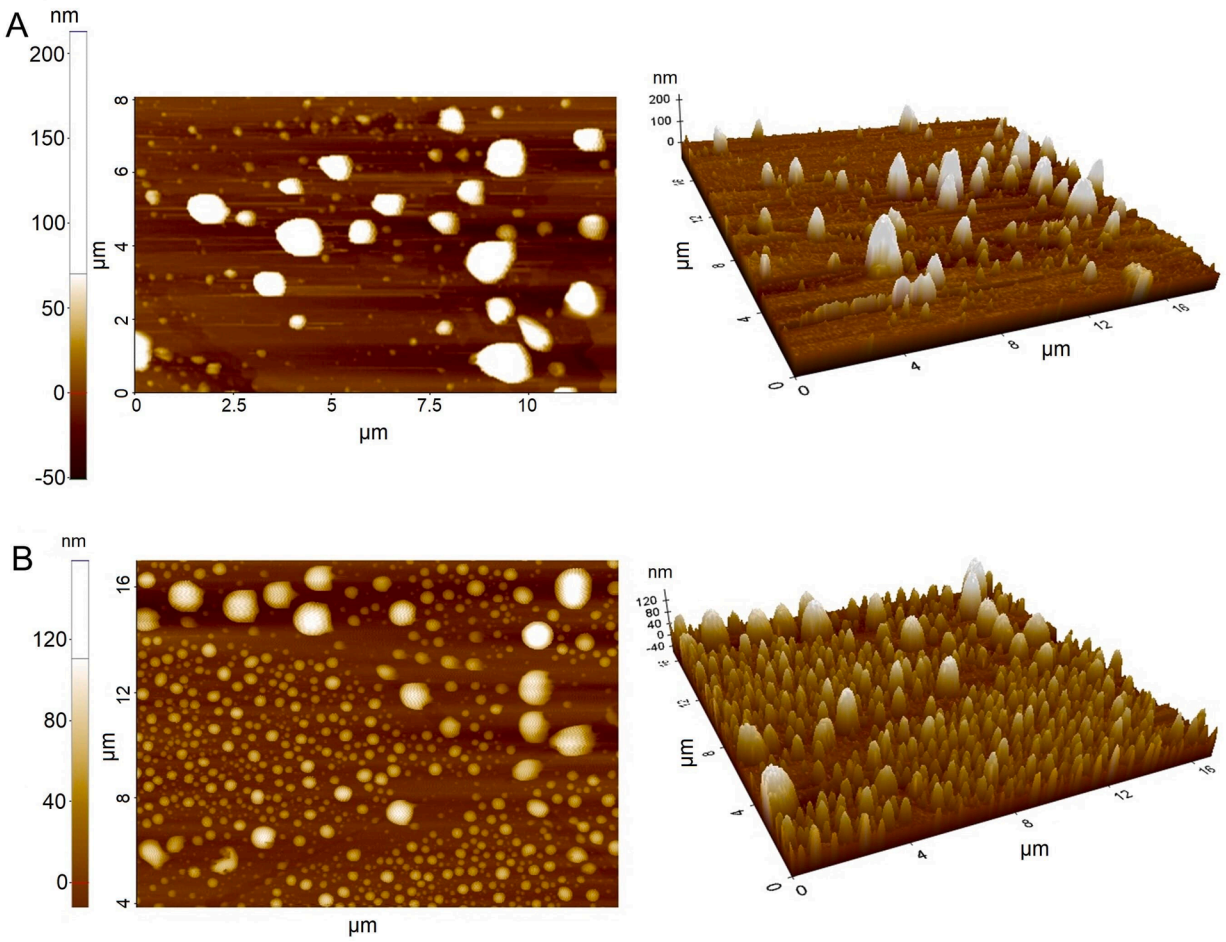

Fig. 3. AFM images of unloaded-NLC (A) and CBD-NLC (B): 2D surface topography and 3D particle distribution.

2.9.7. Statistical analysis

The in vivo data are presented as the mean ± *S*.E.M. of the evaluated parameter and were analysed by two-way ANOVA for repeated measurements, followed by Bonferroni's post-hoc test for multiple comparisons. The minimum level of significance was set at $p < 0.05$. Statistical analyses and figure preparation were performed using version 5 of GraphPad Prism (GraphPad Software, La Jolla, CA).

3. Results and discussion

3.1. Preparation and characterisation of NLC

In this study, we developed a mucoadhesive NLC for the nasal administration of CBD. One of the strategies employed was to develop positively charged particles. For this, a cationic surfactant (cetylpyridinium chloride) was used as a stabiliser, and Span 20® was employed as a co-stabiliser. The NLCs were characterised by their average particle size, PdI, zeta potential, EE, and DL.

Both the unloaded-NLC and CBD-NLC showed nanometric hydrodynamic sizes (285 ± 5.2 nm and 177 ± 3.1 nm, respectively); however, the incorporation of the drug caused a significant decrease in particle size ($p \leq 0.05$, Student's test). This may be related to the lipophilic characteristics of CBD making the system more compact because of the intermolecular interactions that probably occur between CBD and the nonpolar components of the NLC, leading to the retraction of the particles and a decrease in particle size. Regarding PdI, values of 0.34 ± 0.05 and 0.30 ± 0.02 were obtained for the unloaded-NLC and CBD-NLC, respectively, demonstrating homogeneity.

The CBD-NLC showed 99.99% EE (± 0.0001) and 18.75% (± 0.0001) DL, which is attributed to the highly lipophilic nature of the drug (Mendes et al., 2019; Pires et al., 2019). In addition, the NLCs could encapsulate large amounts of the drug because of their disorganised lipid matrix (Khosa et al., 2018; Haider et al., 2020).

Zeta potential is a parameter that influences the physical stability of nanocarriers. It is related to the surface charge of nanoparticles and indicates the degree of repulsion between them. Particle aggregation is less likely in systems with zeta potential values above |30| mV (Müller et al., 2000; Rouco et al., 2020). Zeta potential values of 40 ± 0.5 mV and 41 ± 0.6 mV were obtained for the unloaded-NLC and CBD-NLC, respectively, showing the physical stability of the system. Moreover, the most important feature of these positive zeta potentials is the mucoadhesive properties of the nanoparticles, owing to the possibility of electrostatic interactions with negatively charged mucin (Hommoss et al., 2017; Karimi et al., 2018).

Mucin is known to be a large, negatively charged glycoprotein and is the main macromolecular component of the secretions present on the surface of the nasal mucosa (Akilo et al., 2019; Karimi et al., 2018). Therefore, the positively charged CBD-NLC particles are expected to have a longer retention time on the mucosal surface owing to electrostatic interactions with the oppositely charged mucin. To assess the interactions between the mucin and the CBD-NLC particles, CBD-NLC dispersions were mixed with mucin solutions of different concentrations (0.025–5 mg•mL^{-1}) and the zeta potentials of the NLC particles measured (Fig. 2). Increasing the concentration of mucin added to the NLC dispersions (0.025–0.25 mg•mL^{-1}) led to a decrease in the zeta potential of the NLC particles, indicating interactions with the mucin. Further increases in the concentration of mucin resulted in the charge reversal of the particles, owing to the increased adsorption of negatively

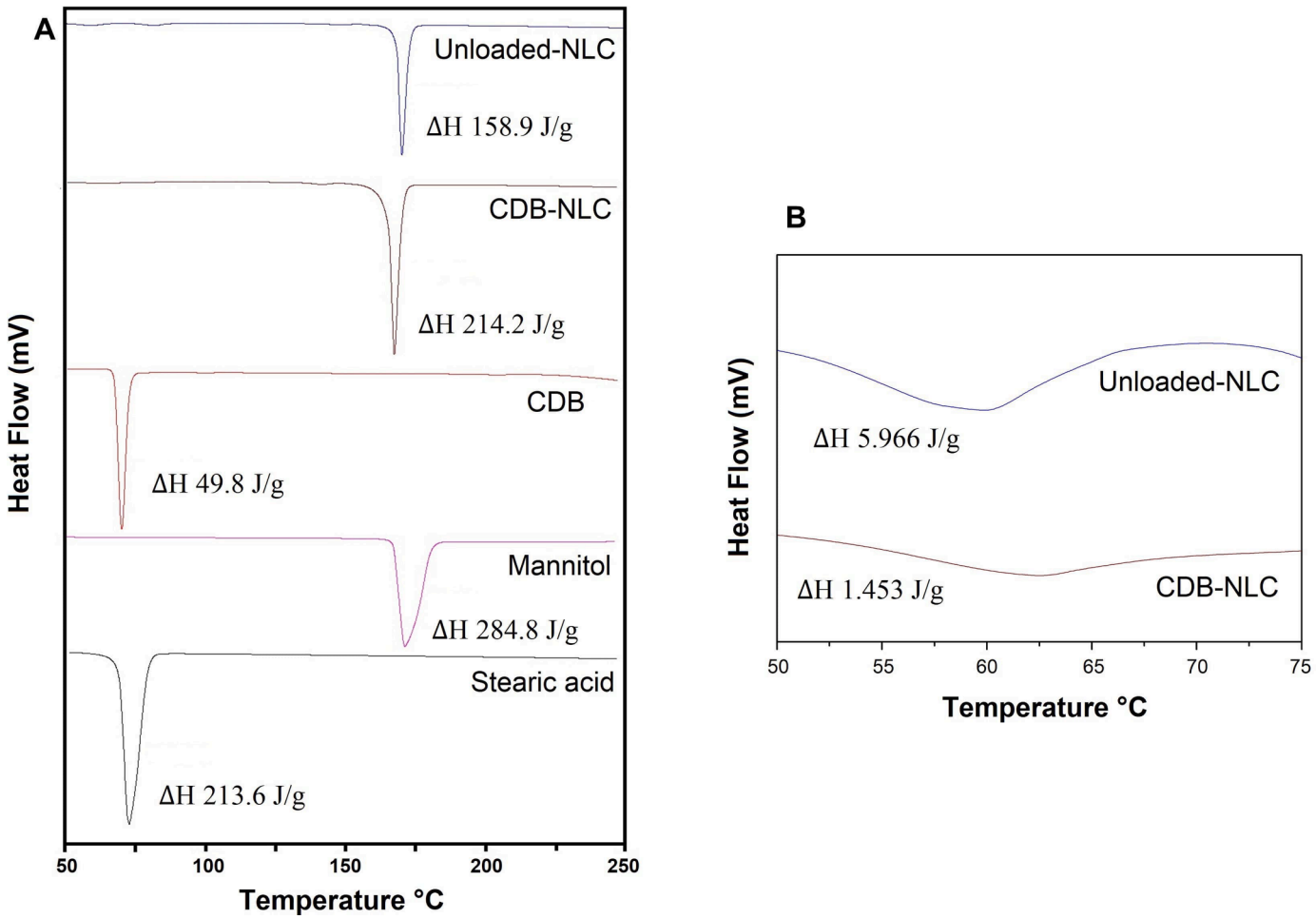

Fig. 4. DSC curves of unloaded-NLC, CBD-NLC, CBD, mannitol, and stearic acid (A). Magnification of the unloaded-NLC and CBD-NLC DSC curves (B). ΔH: enthalpy.

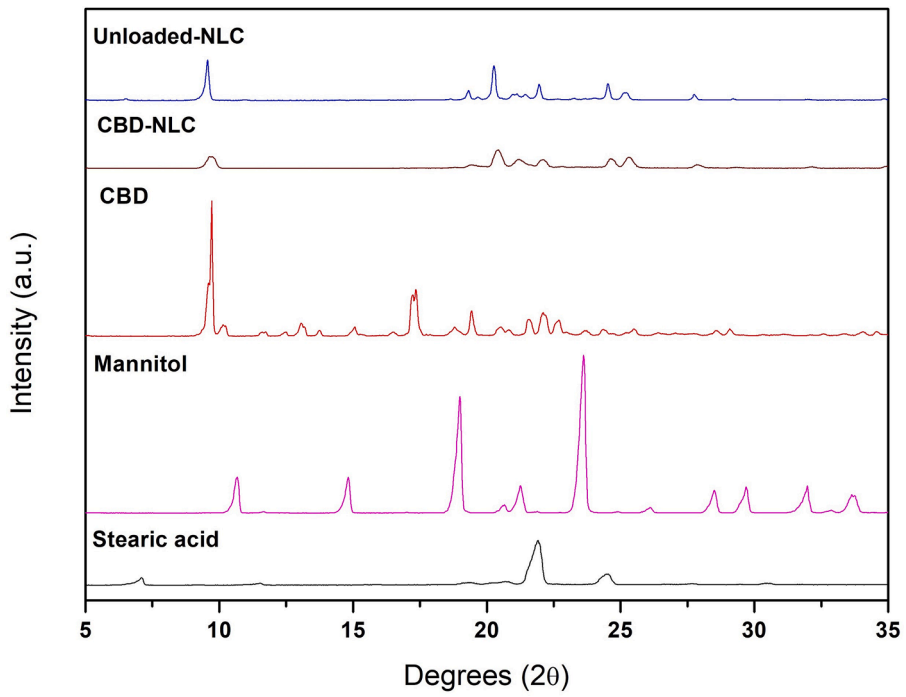

Fig. 5. PXRD patterns of unloaded-NLC, CBD-NLC, CBD, mannitol, and stearic acid.

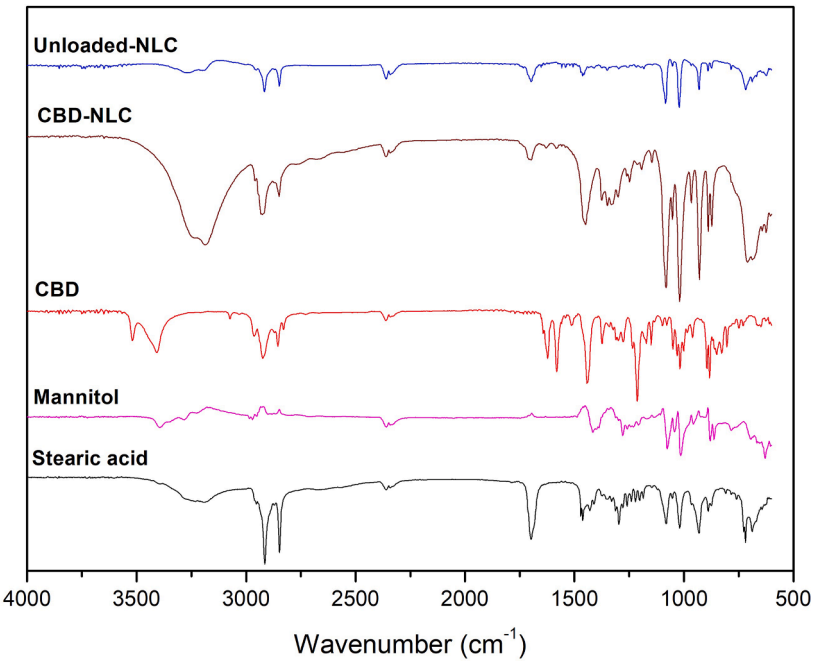

Fig. 6. FTIR-attenuated total reflectance spectra of unloaded-NLC, CBD-NLC, CBD, mannitol, and stearic acid.

charged mucin on the NLC surfaces (Hommoss et al., 2017). These results suggest that CBD-NLC may adhere to the nasal mucosa, increasing the contact time of the formulation in the nasal cavity and improving the bioavailability of the drug.

The unloaded-NLC and CBD-NLC were examined by AFM, and the images are shown in Fig. 3. The NLCs have a spherical shape and a smooth and regular surface. In addition, the AFM results demonstrate that the size of the NLCs was slightly smaller than that observed by the DLS technique. This was caused by methodological differences in size measurement. According to Singh et al. (2016), the DLS technique measures the hydrodynamic particle size, which is always larger than the actual size. Examining the AFM 3D images, we can see that the unloaded-NLC (Fig. 3A) have a maximum roughness of 200 nm, while the CBD-NLC (Fig. 3B) have a roughness of around 80–120 nm. This difference in size between the unloaded-NLC and CBD-NLC corroborates the values obtained in the DLS.

The characterisation of the crystallinity of NLCs is important because it can influence encapsulation and drug release (Attama, 2006; Santos et al., 2019). DSC studies were performed to obtain information about the crystallinity of the NLCs and the interactions between the drug and lipids in the formulation. Fig. 4A shows the DSC curves for stearic acid, CBD, CBD-NLC, unloaded-NLC, and mannitol. The DSC curves of stearic acid, CBD, and mannitol show a single endothermic event at 69.7, 71.8, and 169.7 °C, respectively, which corresponds to the melting points of these compounds, according to the literature (Sallam et al., 2016; Mendes et al., 2019). The DSC curves of the unloaded-NLC and CBD-NLC show a significant event at 169.6 °C, consistent with the melting point of mannitol (used as a cryoprotectant in the freeze-drying process). The NLC melting points were displaced to lower temperatures (59.8 °C in the unloaded-NLC and 62.0 °C in the CBD-NLC) than that of stearic acid, with a significant decrease in enthalpies (Fig. 4B). This could be indicative of the smaller particle size and the reduction in crystallinity attributed to the formation of the NLC matrix, which is composed of a mixture of solid and liquid lipids (Jain et al., 2015; Chauham et al., 2020). Moreover, the CBD-NLC presented a lower melting enthalpy than the unloaded-NLC, which corroborates the DLS and AFM particle size measurements. In addition, the DSC curve of the CBD-NLC did not show a thermal event that could be attributed to the melting of CBD, suggesting that the drug is in an amorphous state or is molecularly dispersed in the lipid matrix.

The crystallinity of the NLCs was also assessed by powder X-Ray diffraction (PXRD). Fig. 5 shows the comparative diffractograms of stearic acid, mannitol, CBD, CBD-NLC, and unloaded-NLC. The main peaks found for stearic acid (7.08°, 11.5°, 19.42°, 20.72°, 21.9°, 24.48°, 27.66°, and 30.52° 2θ), mannitol (10.66° 14.82°, 19.0°, 20.66°, 21.28°, 23.6°, 26.1°, 28.48°, 29.68°, 31.96°, and 33.66° 2θ), and CBD (9.72°, 10.16°, 11.6°, 13.08°, 15.04°, 17.34°, 18.78°, 19.42°, 20.58°, 21.6°, 22.14°, 22.7°, 23.66°, 24.38°, 25.54°, 28.62°, and 29.12° 2θ) show that these compounds have a crystalline nature. The unloaded-NLC and CBD-NLC standards showed similarities. However, the CBD-NLC diffractogram showed a widening of the peaks with displacement to the right. This was probably caused by the presence of CBD in an amorphous state within the lipid matrix, disturbing the crystallinity and decreasing the peak intensity (Müller et al., 2002; Haider et al., 2020). In addition, the absence of CBD peaks (9.72°, 11.6°, and 15.28°) in the CBD-NLC agree with the DSC results, corroborating that the drug is distributed in an amorphous state or molecularly dispersed in the lipid matrix.

FTIR is a technique used to investigate the structural characteristics of lipids and to determine the interactions between a drug and the excipients used in formulations (Mehnert and Mäder, 2012; Kar et al., 2017; Özdemir et al., 2019). The FTIR spectra are shown in Fig 6. The FTIR spectra of mannitol, stearic acid, and CBD are compatible with their structures and consistent with the literature (Duarte, 2016; Zhang et al., 2017; Salyan and Suresh, 2018). In the unloaded-NLC and CBD-NLC spectra, the bands observed are largely consistent with the bands found in the stearic acid and mannitol spectra. Moreover, high-intensity bands of CBD (at 1213 cm^{-1}, 1582 cm^{-1}, 1622 cm^{-1}, 3408 cm^{-1}, and 3520 cm^{-1}) were not observed in the unloaded-NLC and CBD-NLC spectra. Another notable result is the high similarity between the two nanocarrier spectra (unloaded-NLC and CBD-NLC). This similarity could be attributed to the incorporation of the drug into the particle, which occurs by mechanical entrapment. Intermolecular interactions amongst the components of the formulation and the drug may occur, but if so, they are too small to be detected by infrared spectroscopy. The absence of characteristic CBD bands in the CBD-NLC spectrum and the similarity between the unloaded-NLC and CBD-NLC spectra may indicate the absence of free drug on the surface of the nanocarriers (El Assay et al., 2019; Managuli et al., 2019; Mendes et al.,

Table 1
Texture and mucoadhesive strength parameters measured by the texture profile analysis.

Sample	Compressibility (Ns)	Adhesion (Ns)	Cohesion	Hardness (N)	Mucoadhesion
NLC-gel	0.440 ± 0.100 a	0.240 ± 0.040 a	0.720 ± 0.020 a	0.035 ± 0.002 a	0.100 ± 0.001
Chitosan hydrogel	0.250 ± 0.010 b	0.220 ± 0.005 a, b	0.780 ± 0.030 a, b	0.020 ± 0.002 b	0.017 ± 0.001
HPMC hydrogel	0.230 ± 0.002 b, c	0.130 ± 0.015 c	0.830 ± 0.050 b, c	0.020 ± 0.008 b, c	0.017 ± 0.001

NLC, nanostructured lipid carrier; HPMC, hydroxypropyl methylcellulose. Values are expressed as mean ± standard deviation ($n = 3$). Values with different letters in the same column are statistically different according to one-way ANOVA, followed by the Tukey test * $p < 0.05$, $p < 0.01$.

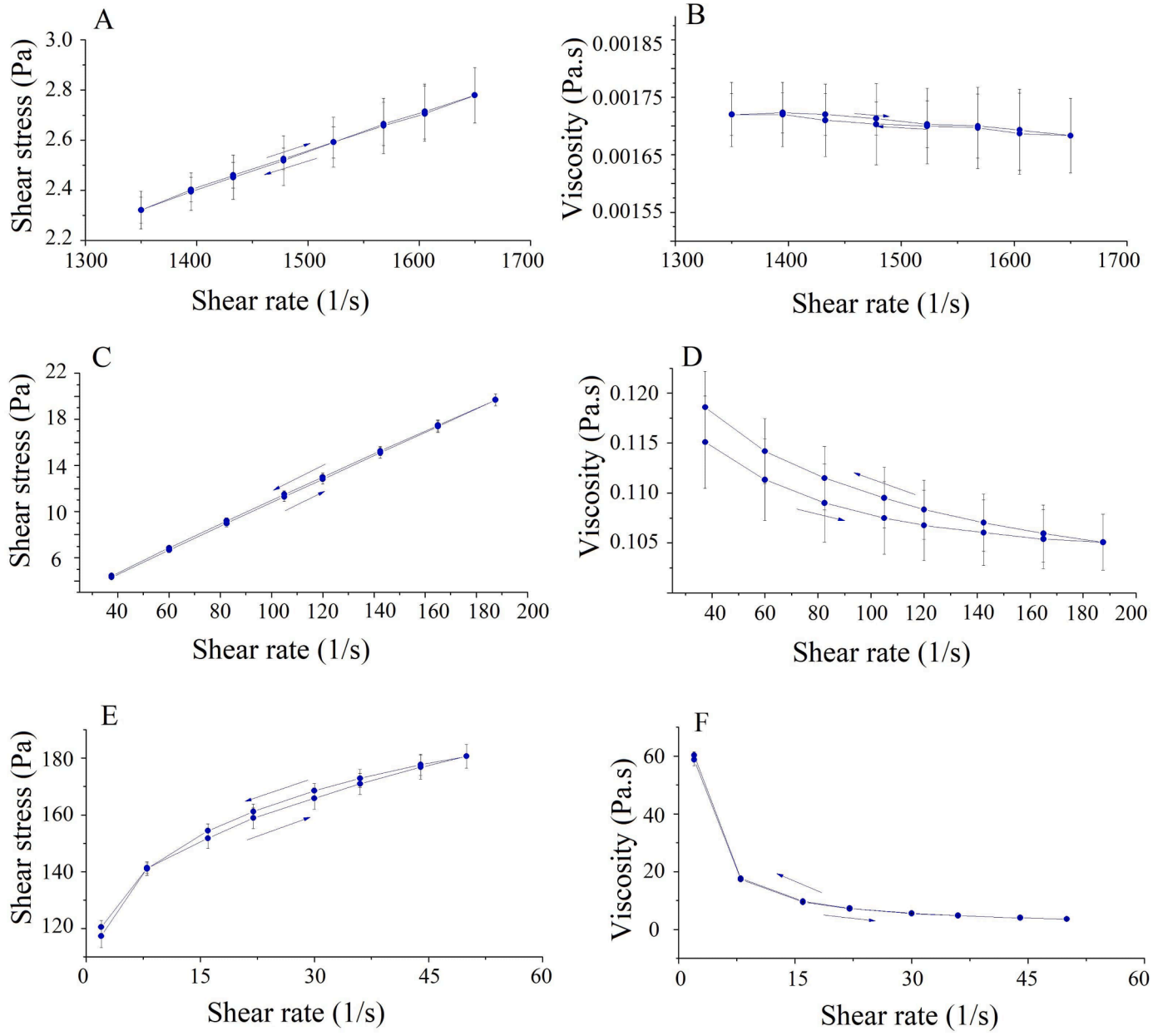

Fig. 7. Flow properties of NLC (A and B), NLC-gel at 25 °C (C and D), and NLC-gel at 37 °C (E and F); $n = 3$.

2019).

3.2. Preparation and characterisation of the NLC-gels

The NLC dispersion was mixed with thermo-reversible polymers to obtain an *in-situ* gelling vehicle when administered to the nasal mucosa, which would be triggered by increasing temperature in vivo. By administering the formulation in a gelling vehicle, an increase in the residence time of the drug in the nasal cavity may occur owing to the increased viscosity of the formulation (Ahmed et al., 2019). Thus, the addition of different proportions of Pluronic F127® and Pluronic F68®, and their behaviour under increasing temperatures, were evaluated. The formulation containing 20% mixed polymers (Pluronic®) at a ratio of 17:3 (Pluronic F127®: Pluronic F68®) showed *Ti* at 34 °C and *Tg* at 37 °C; thus gelation was observed at a temperature close to the temperature of the nasal cavity.

Table 2
Rheological data obtained for NLC and NLC-gel, at 25 ° and 37 °C ($n = 3$).

Sample	Temperature (°C)	Flow index	Consistency index (Pa.s)
NLC	25	0.880	0.004
NLC-gel	25	0.830	0.148
NLC-gel	37	0.880	107.676

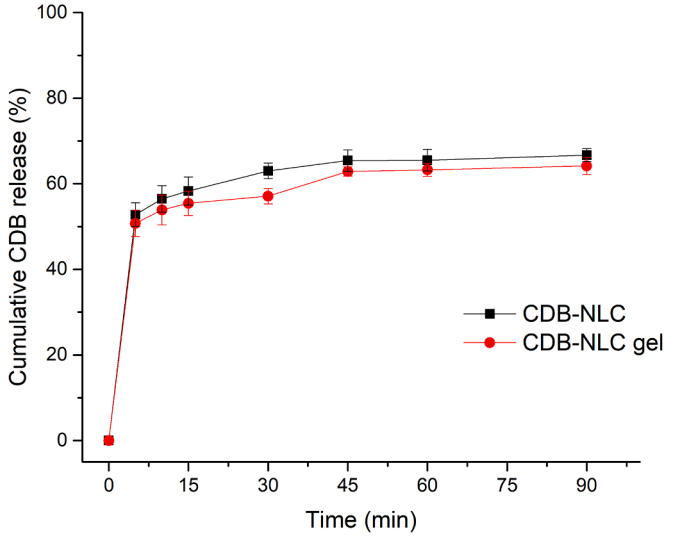

Fig. 8. Cannabidiol (CBD) release profiles from (■) CBD-NLC (as an aqueous dispersion) and (●) CBD-NLC-gel ($n = 6$).

The texture parameters (hardness, compressibility, adhesion, and cohesion) and mucoadhesion strength of the NLC-gel were compared with those obtained for hydrogels of chitosan 5% (w/w) and hydroxypropyl methylcellulose 10% (w/w). The results are shown in Table 1. The NLC-gel showed greater compressibility, hardness, and adhesion than the chitosan or hydroxypropyl methylcellulose hydrogels. Considering that the increased stiffness is related to greater adhesion, we can infer high potential bioadhesion of the NLC-gel. In addition, the tensile strength mucoadhesion measurements also show that the NLC-gel had higher mucoadhesion than the other hydrogels.

The mucoadhesive properties of the CBD-NLC and CBD-NLC-gel were also determined by the flow-through method. This method is often employed for dosage forms administered via the intranasal pathway because nasal mucociliary clearance is an issue still to be solved (Jiang et al., 2017). The amount of CBD retained on the mucosa was 64.5% from the CBD-NLC, 78.8% from the CBD-NLC-gel, and 35.3% from the drug solution (control). These results are important to demonstrate that mucoadhesion of the CBD-NLC occurred as a function of electrostatic interactions with mucin, while the mucoadhesion of the CBD-NLC-gel is dependant on *in-situ* gelling.

Rheological analyses were performed for NLC dispersion and NLC-gel at 25 °C and 37 °C, and the results are shown in Fig. 7. The NLC dispersion showed Newtonian flow ($\eta = 1$), while the NLC-gel showed pseudoplastic ($\eta < 1$) and thixotropic flow. In addition, the NLC-gel showed a higher consistency index at 37 °C than at 25 °C (Table 2), related to the gelling agent and leading to an increase in the apparent viscosity of the formulation. This rheological behaviour of the NLC-gel is desirable considering that, at room temperature, the formulation has low viscosity, facilitating application and spreadability at the application site. However, when applied to the nasal mucosae, the apparent viscosity of the NLC-gel increases at a normal human body temperature. The increased viscosity of the NLC-gel after administration to the nasal mucosae contributes to the mucoadhesiveness of the formulation.

In vitro drug release studies were performed with CBD-NLC and CBD-NLC-gel, and the results are shown in Fig. 8. The release profiles of CBD from the two formulations showed an initial burst (releasing more than 50% of the drug in 5 min), followed by slow and sustained release. This biphasic release pattern has been previously observed for NLCs (Bhadra et al., 2017; Garg et al., 2017; Pivetta et al., 2018; Mendes et al., 2019) and has been related to drug diffusion from the lipid matrix of the NLCs, and to drug location in the lipid matrix. During NLC preparation, the

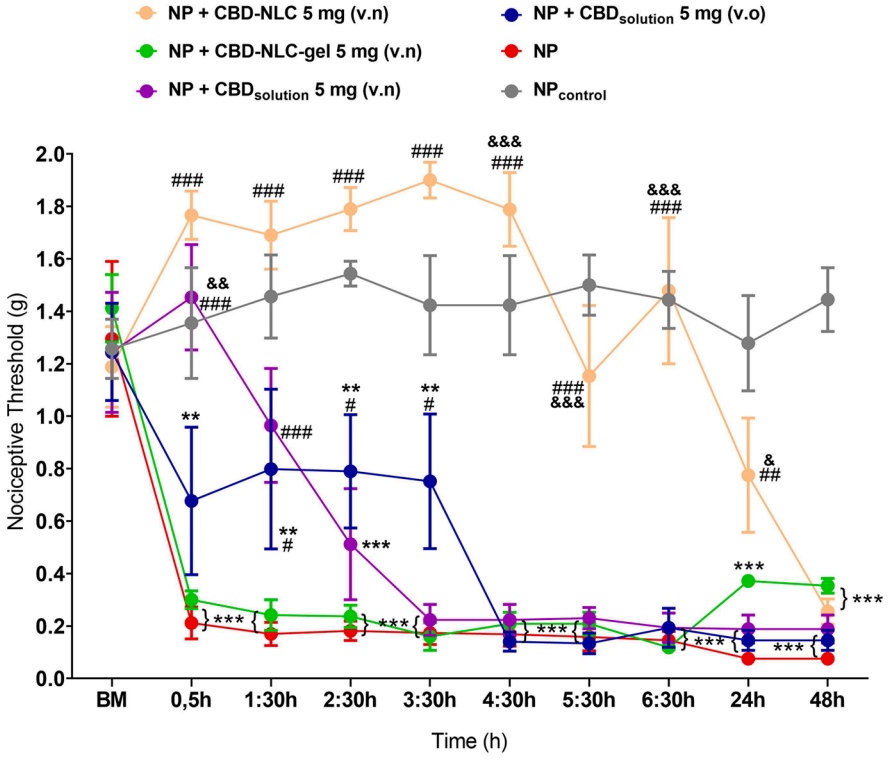

Fig. 9. Effect of different formulations with cannabidiol (CBD) and different treatment routes on the nociceptive threshold of mice with PTX-induced neuropathic pain (NP). Before the induction of NP, a baseline measurement of the nociceptive threshold (MB) was performed in each animal. Then new measurements were taken on the 14th day of pain. The animals received CBD solution (5 mg•kg^{-1}) intranasally (v.n) and orally (v.o), CBD-NLC (equivalent to 5 mg•kg^{-1} of CBD) v.n, and CBD-NLC-gel (equivalent to 5 mg•kg^{-1} of CBD) v.n. Data are presented according to the mean + SEM of the nociceptive threshold of six animals per group. *** $p < 0.001$: statistical difference between the group of animals with NP and control animals; # $p < 0.05$, ## $p < 0.01$, and ### $p < 0.01$: statistical differences between the group of animals with NP and the groups of animals with NP + CBD treatment; and & $p < 0.05$, && $p < 0.01$, and &&& $p < 0.001$: statistical differences between groups of animals with NP that received CBD v.o versus groups of animals with NP that received CBD v.n or CBD-NLC v.n. Two-way ANOVA followed by Bonferroni's post-hoc test.

rapid cooling of the lipids favours enrichment of the drug in the outer layers of the nanocarriers. This superficial entrapment leads to an initial burst release (Kar et al., 2017). The sustained release pattern of CBD could be attributed to strong interactions with the lipid matrix because of its high lipophilicity, as well as the slow degradation of the NLCs in the release medium. No differences were observed in the release profiles or amounts of CBD released from the CBD-NLC and CBD-NLC-gel. This is probably because the large volume of medium used in the release studies, instead of leading to the formation of a gelled matrix, caused the dissolution of the polymers.

3.3. In vivo studies

To evaluate the in vivo efficacy of nasal CBD administration from the developed mucoadhesive formulations, CBD-NLC, CBD-NLC-gel, and CBD solution (used as a control) were administered intranasally to mice with PTX-induced neuropathic pain. In addition, oral administration of CBD solution was assessed as a positive control. Mice that underwent PTX-induced neuropathic pain presented with mechanical allodynia that lasted for more than 14 days. (Fig. 3S). Thus, the CBD was administered on the 14th day, when neuropathic pain was already installed. The dose/response experiment found that the CBD oral solution induced antinociception at a dose of 5 $mg \bullet kg^{-1}$ (data not shown).

Nasal administration of CBD-NLC produced a significant antinociceptive effect in animals with neuropathic pain ($p < 0.001$), and this effect lasted for more than 6 h (Fig. 9). Moreover, CBD solution administered through the nasal route produced antinociception ($p < 0.001$); however, this effect lasted only 1 h 30 min. When compared to the oral route, the intranasally administered CBD solution produced a faster effect, demonstrating the ability of the nasal route to transport the drug directly to the brain, possibly overcoming the first hepatic metabolism that occurs after absorption through the gastrointestinal mucosae (Chatterjee et al., 2019; Costa et al., 2019; Akel et al., 2020). Intranasally administered CBD-NLC showed a better antinociception effect than CBD solution, administered intranasally or orally, showing enhanced effectiveness and prolonged effect duration.

However, CBD-NLC-gel administered intranasally did not alter mechanical allodynia ($p > 0.05$). These findings were associated with a reduced in vivo release of CBD, probably owing to the viscosity of the hydrogel formed in situ, which adds an additional diffusional resistance to drug release (Abdeltawab et al., 2020; Pineda-Hernández et al., 2020), and the lipophilic properties of the drug and its limited diffusion through the aqueous medium of the hydrogel. The lipophilicity of CBD makes its release dependant mainly on the dissolution and erosion of the polymeric matrix of the gel. The erosion rate tends to decrease owing to the presence of NLCs in the gel (Nie et al., 2011; Pineda-Hernández et al., 2020). This can hinder the release and absorption of the drug. As expected, neither unloaded-NLC nor unloaded-NLC-gel altered the nociceptive threshold (Fig. 4S)

Neither the CBD-NLC (administered intranasally) nor the CBD solution (administered intranasally and orally) influenced the time of permanence of the animals, as evaluated by motor performance tests (Fig. 5S). These findings indicate that CBD does not have adverse effects on the central nervous system, such as sedation, and confirms that the CBD effects evaluated by the von Frey test were specifically antinociceptive.

4. Conclusion

Mucoadhesive NLC formulations loaded with CBD were developed and characterised. The mucoadhesiveness of the formulations based on cationic CBD-NLC, designated as an aqueous dispersion of these nanocarriers or a CBD-NLC-gel, was characterised by an in vitro assay. The in vitro release studies showed that both formulations exhibited a burst effect, releasing about 50% of their CBD within 5 min. The in vivo performance, assessed by antinociceptive effects following nasal administration of the formulations in mice with chemotherapy-induced neuropathic pain, showed that CBD-NLC as an aqueous dispersion produced a greater antinociceptive effect than nasally or orally administered CBD solution. However, CBD-NLC-gel did not show any antinociceptive effect. Although the NLC-gel increased the residence time of the formulation in the nasal cavity, the viscosity and hydrophilic characteristics of this formulation hindered the diffusion and release of the lipophilic drug, reducing its nasal absorption. Therefore, CBD-NLC, administered as an aqueous dispersion via the nasal route, is a promising delivery system to enhance the bioavailability of CBD in the brain.

CRediT authorship contribution statement

Ananda Pulini Matarazzo: Methodology, Investigation, Writing - original draft. **Lívia Maria Silvestre Elisei:** Investigation. **Flávia Chiva Carvalho:** Supervision. **Rudy Bonfílio:** Methodology, Validation. **André Luís Morais Ruela:** Writing - review & editing. **Giovane Galdino:** Supervision, Writing - review & editing. **Gislaine Ribeiro Pereira:** Project administration, Supervision, Writing - review & editing.

Declaration of Competing Interest

The authors report no conflicts of interest. The authors are responsible for the content of this article.

Acknowledgements

The authors wish to thank Coordenação de Aperfeiçoamento de Pessoal de Nível Superior - Brasil (CAPES) for the financial support (Finance Code 001).

Supplementary materials

Supplementary material associated with this article can be found, in the online version, at doi:10.1016/j.ejps.2020.105698.

References

Abdeltawab, H., Svirskis, D., Sharma, M., 2020. Formulation strategies to modulate drug release from poloxamer based in situ gelling systems. Expert Opin. Drug Deliv. 17 (4), 495–509. https://doi.org/10.1080/17425247.2020.1731469.

Ahmed, S., Gull, A., Aqil, M., Danish Ansari, M., Sultana, Y., 2019. Poloxamer-407 thickened lipid colloidal system of agomelatine for brain targeting: characterization, brain pharmacokinetic study and behavioral study on Wistar rats. Colloids Surfaces B Biointerfaces 181, 426–436. https://doi.org/10.1016/j.colsurfb.2019.05.016.

Akel, H., Ismail, R., Csóka, I., 2020. Progress and perspectives of brain-targeting lipid-based nanosystems via the nasal route in Alzheimer's disease. Eur. J. Pharm. Biopharm. 148, 38–53. https://doi.org/10.1016/j.ejpb.2019.12.014.

Akilo, O.D., Kumar, P., Choonara, Y.E., du Toit, L.C., Pradeep, P., Modi, G., Pillay, V., 2019. In situ thermo-co-electroresponsive mucogel for controlled release of bioactive agent. Int. J. Pharm. 559, 255–270. https://doi.org/10.1016/j.ijpharm.2019.01.044.

Beloqui, A., Solinís, M.Á., Rodríguez-Gascón, A., Almeida, A.J., Préat, V., 2016. Nanostructured lipid carriers: promising drug delivery systems for future clinics. Nanomed. Nanotechnol. 12, 143–161. https://doi.org/10.1016/j.nano.2015.09.004. Biol. Med.

Bhadra, A., Karmakar, G., Nahak, P., Chettri, P., Roy, B., Guha, P., Mandal, A.K., Nath, R. K., Panda, A.K., 2017. Impact of detergents on the physiochemical behavior of itraconazole loaded nanostructured lipid carriers. Colloids Surfaces A Physicochem. Eng. Asp. 516, 63–71. https://doi.org/10.1016/j.colsurfa.2016.12.009.

Blanton, H.L., Brelsfoard, J., DeTurk, N., Pruitt, K., Narasimhan, M., Morgan, D.J., Guindon, J., 2019. Cannabinoids: current and future options to treat chronic and chemotherapy-induced neuropathic pain. Drugs 79 (9), 969–995. https://doi.org/10.1007/s40265-019-01132-x.

BRASIL, 2017. RDC Nº 166, de 24 de julho de 2017. Dispõe sobre a validação de métodos analíticos e dá outras providências. Diário Of. [da] República Fed. do Bras 2017, 22.

Brenneman, D.E., Kinney, W.A., Ward, S.J., 2019. Knockdown siRNA targeting the mitochondrial sodium-calcium exchanger-1 inhibits the protective effects of two cannabinoids against acute paclitaxel toxicity. J. Mol. Neurosci. 68 (4), 603–619. https://doi.org/10.1007/s12031-019-01321-z.

Bruni, N., Pepa, C.Della, Oliaro-Bosso, S., Pessione, E., Gastaldi, D., Dosio, F., 2018. Cannabinoid delivery systems for pain and inflammation treatment. Molecules 23 (10), 2478–2503. https://doi.org/10.3390/molecules23102478.

Chatterjee, B., Gorain, B., Mohananaidu, K., Sengupta, P., Mandal, U.K., Choudhury, H., 2019. Targeted drug delivery to the brain via intranasal nanoemulsion: available proof of concept and existing challenges. Int. J. Pharm. 565, 258–268. https://doi.org/10.1016/j.ijpharm.2019.05.032.

Cherniakov, I., Izgelov, D., Domb, A.J., Hoffman, A., 2017. The effect of Pro NanoLipospheres (PNL) formulation containing natural absorption enhancers on the oral bioavailability of delta-9-tetrahydrocannabinol (THC) and cannabidiol (CBD) in a rat model. Eur. J. Pharm. Sci. 109, 21–30. https://doi.org/10.1016/j.ejps.2017.07.003.

Colombo, M., Figueiro, F., Dias, A.F., Teixeira, H.F., Battastini, A.M.O., Koester, L.S., 2018. Kaempferol-loaded mucoadhesive nanoemulsion for intranasal administration reduces glioma growth in vitro. Int. J. Pharm. 543, 214–223. https://doi.org/10.1016/j.ijpharm.2018.03.055.

Costa, C., Moreira, J.N., Amaral, M.H., Sousa Lobo, J.M., Silva, A.C., 2019. Nose-to-brain delivery of lipid-based nanosystems for epileptic seizures and anxiety crisis. J. Control. Release 295, 187–200. https://doi.org/10.1016/j.jconrel.2018.12.049.

Cunha, S., Amaral, M.H., Sousa Lobo, J.M., Silva, A.C., 2017. Lipid nanoparticles for nasal/intranasal drug delivery. Crit. Rev. Ther. Drug Carrier Syst. 34, 257–282. https://doi.org/10.1615/CritRevTherDrugCarrierSyst.2017018693.

De Gregorio, D., McLaughlin, R.J., Posa, L., Ochoa-Sanchez, R., Enns, J., Lopez-Canul, M., Aboud, M., Maione, S., Comai, S., Gobbi, G., 2019. Cannabidiol modulates serotonergic transmission and reverses both allodynia and anxiety-like behavior in a model of neuropathic pain. Pain 160, 136–150. https://doi.org/10.1097/j.pain.0000000000001386.

Deepak, P., Seema, P., Sarvesh, P., Gargi, P., Swapnil, S., 2019. Nanostructured lipid carriers : a platform to lipophilic drug for oral bioavailability enhancement. J. Drug Deliv. Ther. 9, 758–764. https://doi.org/10.22270/jddt.v9i3-s.2750.

Duarte, P., 2016. Determination of the antibiotic properties of cannabidiol. J. Gen. Pract. 4, 4–6. https://doi.org/10.41072/2329-9126.1000266.

Dunham, N.W., Miya, T.S., 1957. A note on a simple apparatus for detecting neurological deficit in rats and mice. J. Am. Pharm. Assoc. Am. Pharm. Assoc. (Baltim). 46, 208–209. https://doi.org/10.1002/jps.3030460322.

Fasinu, P.S., Phillips, S., ElSohly, M.A., Walker, L.A., 2016. Current status and prospects for cannabidiol preparations as new therapeutic agents. Pharmacotherapy 36, 781–796. https://doi.org/10.1002/phar.1780.

Gadhave, D.G., Kokare, C.R., 2019. Nanostructured lipid carriers engineered for intranasal delivery of teriflunomide in multiple sclerosis: optimization and in vivo studies. Drug Dev. Ind. Pharm. 45, 839–851. https://doi.org/10.1080/03639045.2019.1576724.

Garg, N.K., Sharma, G., Singh, B., Nirbhavane, P., Tyagi, R.K., Shukla, R., Katare, O.P., 2017. Quality by Design (QbD)-enabled development of aceclofenac loaded-nano structured lipid carriers (NLCs): an improved dermatokinetic profile for inflammatory disorder(s). Int. J. Pharm. 517, 413–431. https://doi.org/10.1016/j.ijpharm.2016.12.010.

Gasco, M.R., 1993. Method for producing solid lipid microspheres having a narrow size distribuition. United States Patent 5250236.

Gaston, T.E., Friedman, D., 2017. Pharmacology of cannabinoids in the treatment of epilepsy. Epilepsy Behav 70, 313–318. https://doi.org/10.1016/j.yebeh.2016.11.016.

Haider, M., Abdin, S.M., Kamal, L., Orive, G., 2020. Nanostructured lipid carriers for delivery of chemotherapeutics: a review. Pharmaceutics 12 (3), 288–314. https://doi.org/10.3390/pharmaceutics12030288.

Hanson, L.R., Fine, J.M., Svitak, A.L., Faltesek, K.A., 2013. Intranasal administration of CNS therapeutics to awake mice. J. Vis. Exp. 74, 1–7. https://doi.org/10.3791/4440.

Hommoss, G., Pyo, S.M., Müller, R.H., 2017. Mucoadhesive tetrahydrocannabinol-loaded NLC – Formulation optimization and long-term physicochemical stability. Eur. J. Pharm. Biopharm. 117, 408–417. https://doi.org/10.1016/j.ejpb.2017.04.009.

Jain, K., Sood, S., Gowthamarajan, K., 2015. Optimization of artemether-loaded NLC for intranasal delivery using central composite design. Drug Deliv. 22, 940–954. https://doi.org/10.3109/10717544.2014.885999.

Jiang, W.Z., Cai, Y., Li, H.Y., 2017. Chitosan-based spray-dried mucoadhesive microspheres for sustained oromucosal drug delivery. Powder Technol. 312, 124–132. https://doi.org/10.1016/j.powtec.2017.02.021.

Kar, N., Chakraborty, S., De, A.K., Ghosh, S., Bera, T., 2017. Development and evaluation of a cedrol-loaded nanostructured lipid carrier system for in vitro and in vivo susceptibilities of wild and drug resistant Leishmania donovani amastigotes. Eur. J. Pharm. Sci. 104, 196–211. https://doi.org/10.1016/j.ejps.2017.03.046.

Karimi, N., Ghanbarzadeh, B., Hamishehkar, H., Mehramuz, B., Kafil, H.S., 2018. Antioxidant, antimicrobial and physicochemical properties of turmeric extract-loaded Nanostructured Lipid Carrier (NLC). Colloids Interface Sci. Commun. 22, 18–24. https://doi.org/10.1016/j.colcom.2017.11.006.

Khosa, A., Reddi, S., Saha, R.N., 2018. Nanostructured lipid carriers for site-specific drug delivery. Biomed. Pharmacother. 103, 598–613. https://doi.org/10.1016/j.biopha.2018.04.055.

Managuli, R.S., Wang, J.T., Faruqu, F.N., Kushwah, V., Raut, S.Y., Shreya, A.B., Al-Jamal, K.T., Jain, S., Mutalik, S., 2019. Asenapine maleate-loaded nanostructured lipid carriers: optimization and in vitro, ex vivo and in vivo evaluations. Nanomedicine 14, 889–910. https://doi.org/10.2217/nnm-2018-0289.

Martins, P.P., Smyth, H.D.C., Cui, Z., 2019. Strategies to facilitate or block nose-to-brain drug delivery. Int. J. Pharm. 570, 118635 https://doi.org/10.1016/j.ijpharm.2019.118635.

Mehnert, W., Mäder, K., 2012. Solid lipid nanoparticles: production, characterization and applications. Adv. Drug Deliv. Rev. 64, 83–101. https://doi.org/10.1016/j.addr.2012.09.021.

Mendes, I.T., Ruela, A.L.M., Carvalho, F.C., Freitas, J.T.J., Bonfilio, R., Pereira, G.R., 2019. Development and characterization of nanostructured lipid carrier-based gels for the transdermal delivery of donepezil. Colloids Surfaces B Biointerfaces 177, 274–281. https://doi.org/10.1016/j.colsurfb.2019.02.007.

Müller, R.H., Mäder, K., Gohla, S., 2000. Solid lipid nanoparticles (SLN) for controlled drug delivery - a review of the state of the art. Eur. J. Pharm. Biopharm. 50, 161–177. https://doi.org/10.1016/S0939-6411(00)00087-4.

Müller, R.H., Radtke, M., Wissing, S.A., 2002. Nanostructured lipid matrices for improved microencapsulation of drugs. Int. J. Pharm. 242, 121–128. https://doi.org/10.1016/S0378-5173(02)00180-1.

Nie, S., Hsiao, W.W., Pan, W., Yang, Z., 2011. Thermoreversible pluronic® F127-based hydrogel containing liposomes for the controlled delivery of paclitaxel: in vitro drug release, cell cytotoxicity, and uptake studies. Int. J. Nanomed. 6, 151–166. https://doi.org/10.2147/IJN.S15057.

Özdemir, S., Çelik, B., Üner, M., 2019. Properties and therapeutic potential of solid lipid nanoparticles and nanostructured lipid carriers as promising colloidal drug delivery systems, materials for biomedical engineering: nanomaterials-based drug delivery. 457–505 https://doi.org/10.1016/B978-0-12-816913-1.00015-5.

Paudel, K.S., Hammell, D.C., Agu, R.U., Valiveti, S., Stinchcomb, A.L., 2010. Cannabidiol bioavailability after nasal and transdermal application: effect of permeation enhancers. Drug Dev. Ind. Pharm. 36, 1088–1097. https://doi.org/10.3109/03639041003657295.

Pineda-Hernández, M.T., Pérez-Urizar, J.T., Ganem-Rondero, A., 2020. Thermo-reversible in situ forming implant with nanostructured lipid carriers (NLC) as a delivery system for the administration of estradiol valerate. Drug Deliv. Transl. Res. 10, 1393–1402. https://doi.org/10.1007/s13346-019-00704-4.

Pires, F.Q., da Silva, J.K.R., Sa-Barreto, L.L., Gratieri, T., Gelfuso, G.M., Cunha-Filho, M., 2019. Lipid nanoparticles as carriers of cyclodextrin inclusion complexes: a promising approach for cutaneous delivery of a volatile essential oil. Colloids Surfaces B Biointerfaces 182, 110382–110390. https://doi.org/10.1016/j.colsurfb.2019.110382.

Pivetta, T.P., Simões, S., Araújo, M.M., Carvalho, T., Arruda, C., Marcato, P.D., 2018. Development of nanoparticles from natural lipids for topical delivery of thymol: investigation of its anti-inflammatory properties. Colloids Surfaces B Biointerfaces 164, 281–290. https://doi.org/10.1016/j.colsurfb.2018.01.053.

Rouco, H., Diaz-Rodriguez, P., Remuñán-López, C., Landin, M., 2020. Recent advances in solid lipid nanoparticles formulation and clinical applications. Nanomater. Clin. Appl. INC.213-247 https://doi.org/10.1016/b978-0-12-816705-2.00007-2.

Ruela, A.L.M., Carvalho, F.C., Pereira, G.R., 2016. Exploring the phase behavior of monoolein/oleic acid/water systems for enhanced donepezil administration for alzheimer disease treatment. J. Pharm. Sci. 105, 71–77. https://doi.org/10.1016/j.xphs.2015.10.016.

Sallam, M.A., Helal, H.M., Mortada, S.M., 2016. Rationally designed nanocarriers for intranasal therapy of allergic rhinitis: influence of carrier type on in vivo nasal deposition. Int. J. Nanomed. 11, 2345–2357. https://doi.org/10.2147/IJN.S98547.

Salyan, S., Suresh, S., 2018. Study of thermo-physical properties and cycling stability of D-mannitol-copper oxide nanocomposites as phase change materials. J. Energy Storage 15, 245–255. https://doi.org/10.1016/j.est.2017.10.013.

Santos, V.S., Badan, A.P.R., Santana, M.H.A., 2019. Solid lipid nanoparticles as carriers for lipophilic compounds for applications in foods. Food Res. Int. 122, 610–626. https://doi.org/10.1016/j.foodres.2019.01.032.

Sekiguchi, F., Domoto, R., Nakashima, K., Yamasoba, D., Yamanishi, H., Tsubota, M., Wake, H., Nishibori, M., Kawabata, A., 2018. Paclitaxel-induced HMGB1 release from macrophages and its implication for peripheral neuropathy in mice: evidence for a neuroimmune crosstalk. Neuropharmacology 141, 201–213. https://doi.org/10.1016/j.neuropharm.2018.08.040.

Shen, J., Wang, Y., Ping, Q., Xiao, Y., Huang, X., 2009. Mucoadhesive effect of thiolated PEG stearate and its modified NLC for ocular drug delivery. J. Control. Release 137, 217–223. https://doi.org/10.1016/j.jconrel.2009.04.021.

Singh, S., Dadhania, P., Vuddanda, P.R., Jain, A., Velaga, S., 2016. Intranasal delivery of asenapine loaded nanostructured lipid carriers: formulation, characterization, pharmacokinetic and behavioural assessment. RSC Adv. 6, 2032–2045. https://doi.org/10.1039/c5ra19793g.

Starobova, H., Vetter, I., 2017. Pathophysiology of chemotherapy-induced peripheral neuropathy. Front. Mol. Neurosci. 10, 1–21. https://doi.org/10.3389/fnmol.2017.00174.

Zhang, X., Yin, Z., Meng, D., Huang, Z., Wen, R., Huang, Y., Min, X., Liu, Y., Fang, M., Wu, X., 2017. Shape-stabilized composite phase change materials with high thermal conductivity based on stearic acid and modified expanded vermiculite. Renew. Energy 112, 113–123. https://doi.org/10.1016/j.renene.2017.05.026.

Zimmermann, M., 1983. Ethical guidelines for investigations of experimental pain in conscious animals. Pain 16, 109–110. https://doi.org/10.1016/0304-3959(83)90201-4.